Chapter 4

Journal of Molecular Structure 1316 (2024) 139042

Contents lists available at ScienceDirect

Journal of Molecular Structure

journal homepage: www.elsevier.com/locate/molstr

Deciphering the complexation processes of creatinine-cobalt and creatinine-cobalt-2-nitrobenzaldehyde: Morphological, spectroscopic and electrochemical analysis

Nayab Hussain, Panchanan Puzari *

Department of Chemical Sciences, Tezpur University, Napaam, Tezpur, Assam 784028, India

Deciphering the complexation processes of creatinine-cobalt and creatinine-cobalt-2-nitrobenzaldehyde: Morphological, spectroscopic and electrochemical analysis

Highlights

Bringing creatinine, cobalt ion and 2-nitrobenzaldehyde together opens up multiple reaction possibilities. In this chapter, the effect of 2-nitrobenzaldehyde on a new complexation pathway of creatinine-cobalt has been explored, under some controlled conditions. As a result, a 4-coordinated complex, $[Co(CR)_3(H_2O)]Cl_2$, and a 7-coordinated complex, $[Co(CR)_3(H_2O)_2(2\text{-NBA})]Cl_3$, were obtained, where CR = creatinine and 2-NBA = 2-nitrobenzaldehyde. P-XRD analysis confirmed the formation of new amorphous complexes and SEM analysis revealed their rod-shaped and nano-fibrous morphologies respectively. FTIR and Raman analysis established the coordination of cobalt ions with endocyclic nitrogen of creatinine and chelation with the nitro group of 2-NBA. From EDX analysis, close similarities between the experimental and theoretical elemental compositions of the complexes were determined. EPR analysis established the paramagnetic nature of the complexes. While DRS studies indicated different *d*-configurations of the cobalt ions in the complexes, CV and DPV confirmed their respective oxidation states to be +2 and +3. The coordination pathways described here can be put into a creatinine sensor development application.

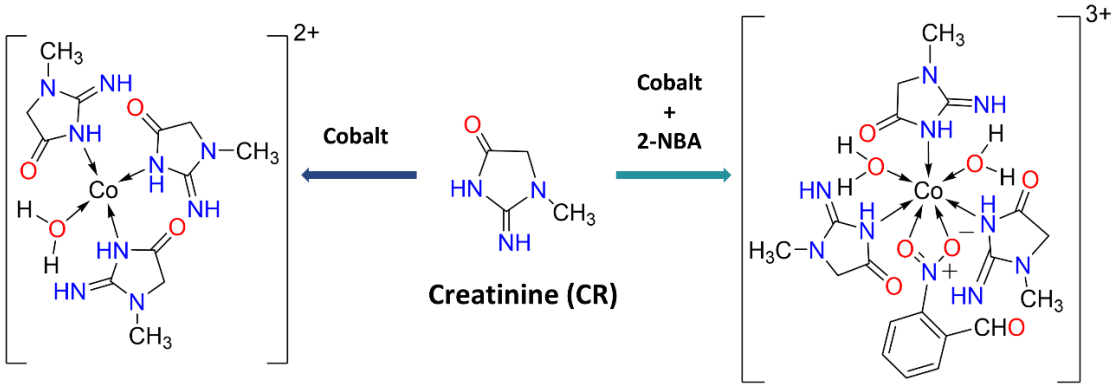

This part of the thesis is published as:

Hussain, N. and Puzari, P. Deciphering the complexation processes of creatinine-cobalt and creatinine-cobalt-2-nitrobenzaldehyde: Morphological, spectroscopic and electrochemical analysis. *Journal of Molecular Structure*, 1316:139042, 2024.

4.1 Introduction

Creatinine has an inherent ability to form complexes with transition metal ions, as discussed in Chapter 1, and it has also been established that the structure and properties of the complexes depend on the solvent system and reaction conditions (pH, temperature, reflux time, etc.) [1]. Although the synthesis of creatinine-transition metal complexes gained prominent attention during the late 20th century, due to their substantial application in creatinine sensor development, researchers continue to tune the conditions and solvent systems to synthesize new creatinine complexes with transition metal ions and other secondary ligands [2-12]. New creatinine complexes with Cu^{2+}, Mn^{2+}, Fe^{3+}, Cr^{3+}, Co^{2+}, Zn^{2+}, Cd^{2+}, Sn^{2+}, Pb^{2+}, and Sb^{2+}, along with their spectroscopic analyses, have been recently reported [10-12].

Apart from the complexation reactions of creatinine with metal ions, its transformation to other products by the action of organic reagents is also vital for sensor applications. As discussed in Chapter 3, *Pilsum et al*. [13] elaborated on the role of 2-nitrobenzaldehyde (2-NBA) in the oxidation of creatinine in the presence of a strong base like NaOH. We optimized this creatinine-oxidation reaction to develop a protocol for a metal-free urinary creatinine level determination [14].

Remarkably, there are also some reports on the ability of the nitrite group to coordinate with metal ions in different ways: coordination via its nitrogen atom to yield nitro-complexes, coordination via one of its oxygen atoms to yield nitrito-complexes, chelation with metal ions via its two oxygen atoms or formation of bridging compounds with two metal ions via its nitrogen atom and one oxygen atom [15, 16]. Many such complexes of Co (II) and Co (III) with the nitrite group were reported [15, 16]. While studying the kinetics of the reaction between p-nitrobenzaldehye and p-toluidine, catalysed by a thiourea complex of Co^{2+}, Eaton et al. [17] anticipated that the catalysis proceeded via coordination of the reactant(s)/intermediate to the metal ion, although no detailed catalytic mechanism has been provided. Furthermore, no literature is available so far highlighting any directly bonded complex of nitrobenzaldehyde and cobalt ions, involving the nitro group. As there are no unshared electrons in the nitrogen atom of nitrobenzaldehyde and it carries a formal charge of +1, the possibility of coordination with

metal ions via the nitrogen atom is ruled out. Nevertheless, the possibility of chelation with the oxygen atoms provides some interesting perspectives.

Thus, from the discussion, it can be comprehended that owing to creatinine's coordinating property with transition metal ions, its oxidation by 2-nitrobenzaldehyde, and the ability of the nitrite group to form chelate and bridging compounds with cobalt ions, different conditions-dependent pathways of reactions are undertaken when any two of the three components (cobalt ion, creatinine, and 2-nitrobenzaldehyde) react. The combination of creatinine, cobalt, and 2-NBA may lead to different reaction pathways. Furthermore, under regulated conditions, new cobalt-creatinine complexes can be synthesized and this chapter focusses on one such new complexation pathway of cobalt and creatinine, in the absence and presence of 2-NBA. Meanwhile, this chapter presents two new complexes of cobalt. Analysis of their SEM images, P-XRD patterns, FTIR spectra, Raman spectra, DRS, EDX spectra, CV, DPV and EPR, enabled us to characterize the complexes and establish their physiochemical differences. This work has also hinted at the possibility of a new electrochemical detection technique for creatinine based on its reaction with the cobalt ion in the presence of 2-NBA.

4.2 Experimental

4.2.1 Chemicals and reagents

Creatinine (98%) was procured from Alfa Aeser, cobalt chloride hexahydrate from Sigma, 2-nitrobenzaldehyde (extrapure analytical reagent) from SRL, ethanol and potassium chloride from Merck. All these chemicals were of analytical reagent grade and used without further purification.

4.2.2 Instrumentation

JSM 6390LV (JEOL, Japan) was used to obtain the SEM images; PXRD patterns were obtained with Bruker D8 ADVANCE ECO P-XRD; FTIR spectra were recorded with PerkinElmer, L1600300 Spectrum TWO LiTa, 91,267, (Llantrisant, UK); RENISHAW basis series with 514 lasers (RENISHAW, UK) was used to record the Raman spectra; Ultraviolet-visible DRS were recorded with UV-2600I (Shimadzu); EDX spectra were recorded with EDX: Model No: 7582 (Oxford make); Electrochemical analysis was carried out with Biologic SP-300-EC-Lab software setup; JES-FA200 (JEOL) was used to

record the EPR; Conductivity measurements were carried out with Systronics conductivity meter (Type: 304, Sr. No. 13,408); lattice parameters were recorded with Bruker AXS SMART APEX-II Single crystal X-ray diffractometer (software: APEX-II).

4.2.3 Synthesis of creatinine-cobalt complexes

4.2.3.1 In the absence of 2-NBA

An aqueous cobalt chloride solution (CCS) of 1 M was prepared by dissolving $CoCl_2 \cdot 6H_2O$ in distilled water. Then, 0.5 mL of CCS was poured over 75 mg of solid creatinine in a beaker. The colourless creatinine crystals at the bottom of the beaker immediately started turning into a dark blue powdery compound (herein to be referred to as C1). C1 was collected after filtration, washed with acetone, dried, and weighed.

4.2.3.2 In the presence of 2-NBA

Two routes were explored as discussed below:

I) Stepwise addition: The first step involved the preparation of C1 as explained above. However, before filtering out C1 from the mixture, 2.5 mL of a 2-NBA solution (7% w/v in ethanol) was added to it. Immediate precipitation, having a dirty-blue appearance, was observed. After sonicating the mixture for 30 s, the precipitate (herein to be referred to as C2) was collected by filtration. C2 was then washed with acetone, dried, and weighed. After drying it was observed that C2 was a mixture of dark blue powder and light blue flakes.

II) Simultaneous addition: In this process, a solution mixture of 0.5 mL 1 M CCS and 2.5 mL 2-NBA (7% w/v in ethanol) was prepared at first. Then, this mixture was poured over 75 mg of creatinine in a beaker. Instant formation of a precipitate (herein to be referred to as C3), having a clear blue appearance, was observed and the mixture was sonicated for 30 s. C3 was collected after filtration, following which it was washed with acetone, dried, and weighed. After drying, it was observed that C3 appeared as light blue flakes.

A brown-coloured filtrate was obtained after filtration in both step-wise and simultaneous addition processes. The filtrate was carefully collected and analyzed separately.

The formation of C1, C2, and C3 are illustrated via Step: A, Step: B, and Step: C respectively, in Figure 4.1. C1, C2, and C3 were recrystallized in distilled water, dried at 100 °C for 6 h, and kept in a vacuum desiccator before proceeding to their characterizations.

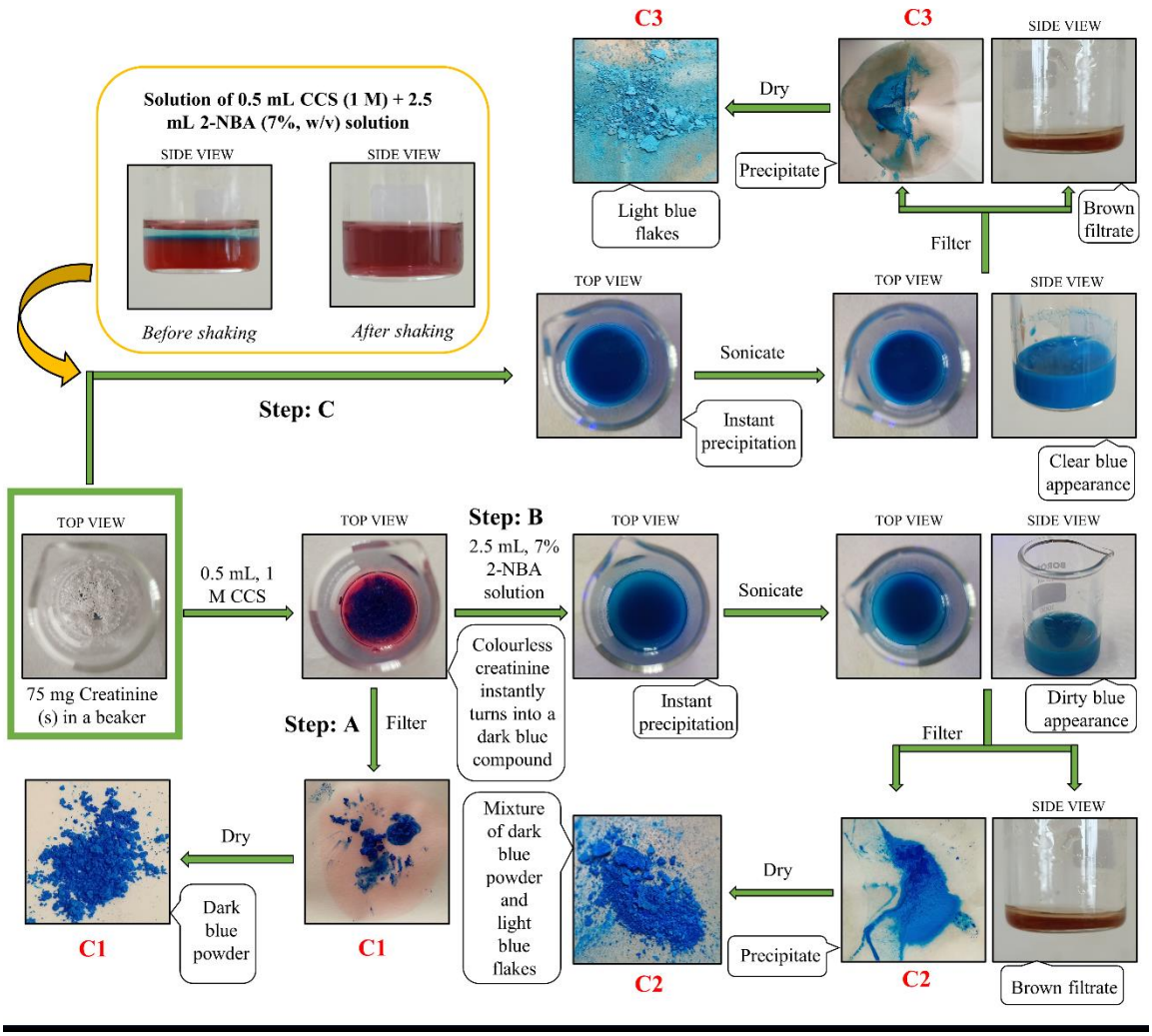

Figure 4.1: Illustration of the processes involved in the synthesis of cobalt complexes.

4.2.4 Microscopic, spectroscopic and physiochemical characterizations

The morphological differences in the complexes were noted by comparing the SEM images at the same magnification (500X). The formation of the new complexes was confirmed by the P-XRD patterns in the 2θ range of 5° to 80°. Evidence on new bond formations and structure of the complexes were gathered from FTIR spectra analysis in

the frequency range of 4000–350 cm^{-1} and Raman spectra analysis in the frequency range of 100 cm^{-1} to 3000 cm^{-1}. The presence of some functional groups and chromophores in the complexes was determined, and the nature of the ligands and *d*-configurations of the central metal ions were inferred by analysing the electronic transitions shown in their DRS (with $BaSO_4$ as the reference standard) in the wavelength range of 200–1400 nm. The elemental compositions of the complexes were determined using EDX spectroscopy and the molecular formulas were deduced. The magnetism of the complexes and the difference in their local environment were established from the EPR spectra. The physical properties like solubility and conductivity of the complexes were also determined.

4.2.5 Electrochemical procedures

CV and DPV techniques were employed for electrochemical analyses. The voltammograms were recorded for aqueous solutions of the synthesized cobalt complexes and compared with the obtained voltammograms for the aqueous solution of $CoCl_2 \cdot 6H_2O$ prepared in distilled water. For CV and DPV, 5 mM $CoCl_2 \cdot 6H_2O$ and 4 mg/ml cobalt-complex solutions were prepared. All the CVs were recorded in the voltage range of − 1.5 V to 1.5 V and with a scan rate of 0.1 V s^{-1}. The DPVs were recorded in the voltage range of − 1.5 V to 1.7 V, with 2.5 mV pulse height, 100 ms pulse width, 5.0 mV step height, and 500.0 ms step time. All the electrochemical analyses were carried out with a bare glassy carbon electrode as the working electrode, Ag/AgCl/KCl (3.5 M) as the reference electrode and a Pt-wire as the counter electrode.

4.3 Results and Discussion

4.3.1 Preliminary observation

The transformation of colourless creatinine crystals to coloured powdery compound, as judged by the naked eye, was either not observed or occurred inefficiently (leaving some colourless creatinine crystals untransformed) when CCS with concentrations of 0.25 M, 0.50 M, and 0.75 M were used. Similarly, with 2-NBA solutions having concentrations of 2 %, 3 %, and 5 %, efficient precipitation was not observed. Hence, the concentration of 1 M CCS and 7 % ethanolic solution of 2-NBA were considered for the reaction. Both complexes were prepared in one-pot synthesis processes.

4.3.2 SEM and P-XRD analysis

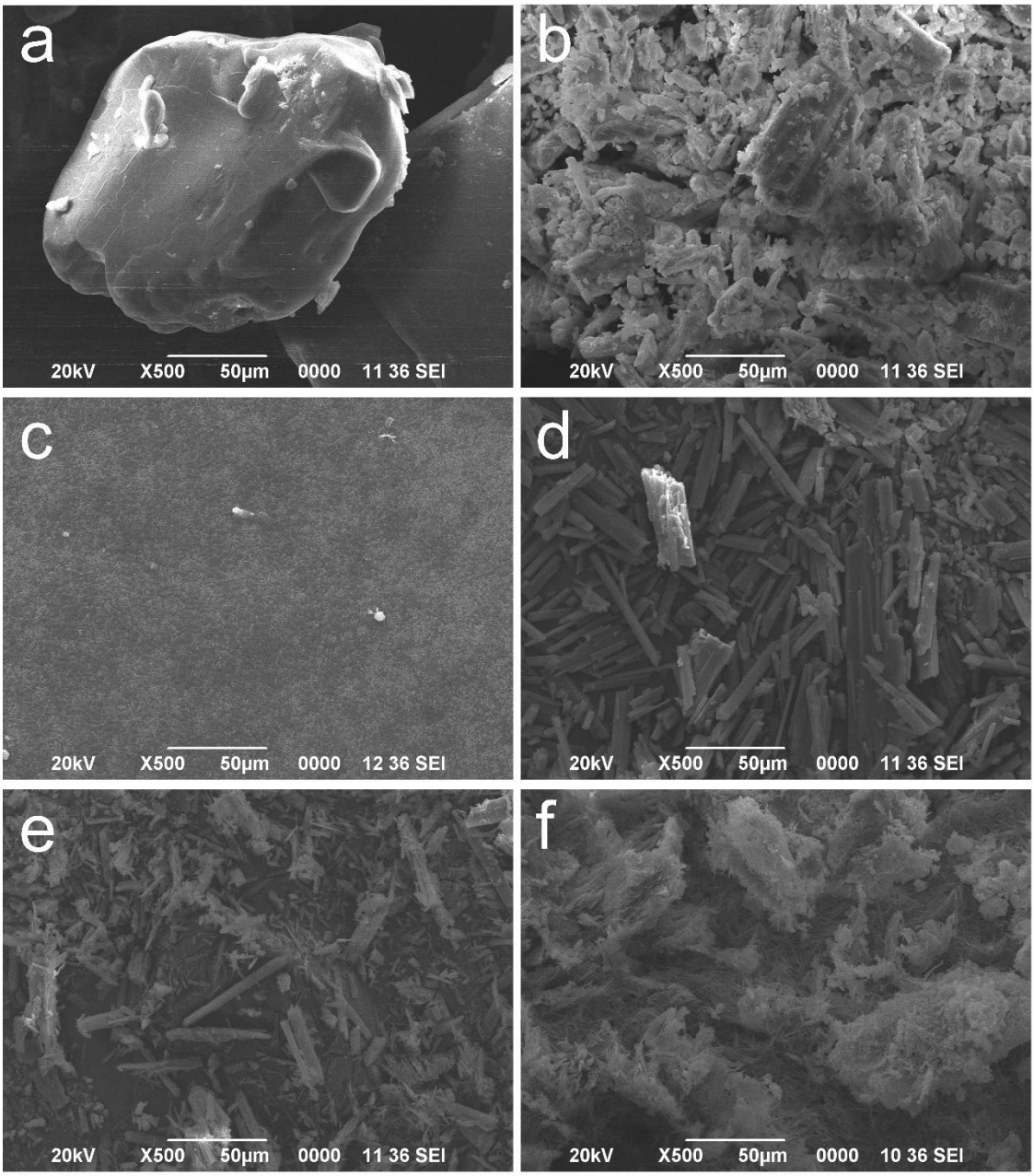

Figure 4.2: SEM image (at X500) of a) creatinine, b) $CoCl_2$ (anhydrous), c) 2-nitrobenzaldehyde, d) C1, e) C2 and f) C3.

As can be seen from the SEM images in Figure 4.2, there are distinct morphological differences between the reactants (a, b, and c) and the formed products (d, e, and f). The SEM image of C1 [Figure 4.2 (d)] revealed a rod-shaped structure for the creatinine-cobalt

complex, but nano-fibrous structures in the case of creatinine-Co-2-NBA [Figure 4.2 (e) and (f)] (structure and formula of the complexes are elucidated in the latter sections).

During the stepwise addition, in the presence of 2-NBA, most of the rod-shaped structures were retained, apart from yielding some nano-fibrous structures, as seen in the SEM image of C2 [Figure 4.2 (e)]. This inferred that the creatinine-cobalt complex produced in the first step was mostly retained even after the addition of 2-NBA in the subsequent step. However, in the case of C3 (simultaneous addition), the SEM image [Figure 4.2 (f)] showed no rod-shaped structures but only nano-fibrous structures. These observations indicated that only a creatinine-cobalt-2-NBA complex was formed during the simultaneous addition process. Furthermore, the SEM images indicated that C2 is a mixture of C1 (dark blue creatinine-cobalt complex) and C3 (light blue creatinine-cobalt-2-NBA complex), which was also apparent during observation with the naked eye.

Some additional SEM images of C1, C2 and C3 at higher magnification are shown in Figure 4.3.

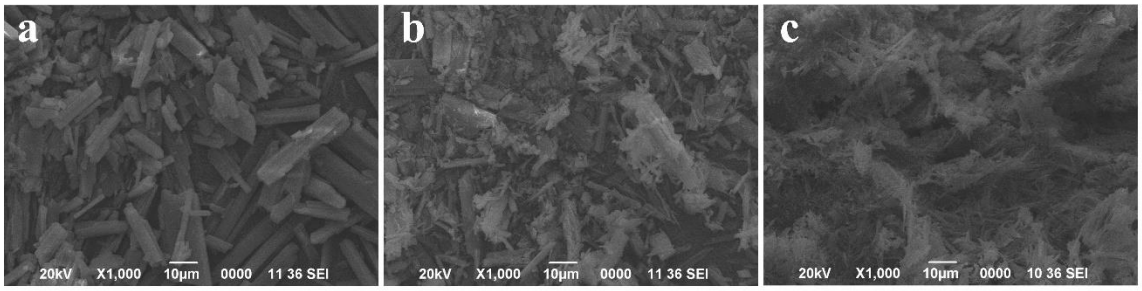

Figure 4.3: SEM images (at X1000) of a) C1, b) C2 and c) C3.

As single crystals could not be obtained, P-XRD patterns were recorded for the reactants and the products as shown in Figure 4.4. Although there is no available report to match the obtained P-XRD pattern of creatinine [Figure 4.4 (a)], the characteristic diffraction patterns obtained for $CoCl_2 \cdot 6H_2O$ [Figure 4.4 (b)] and 2-NBA [Figure 4.4 (c)] matched with their respective diffraction patterns reported in the literature [18, 19].

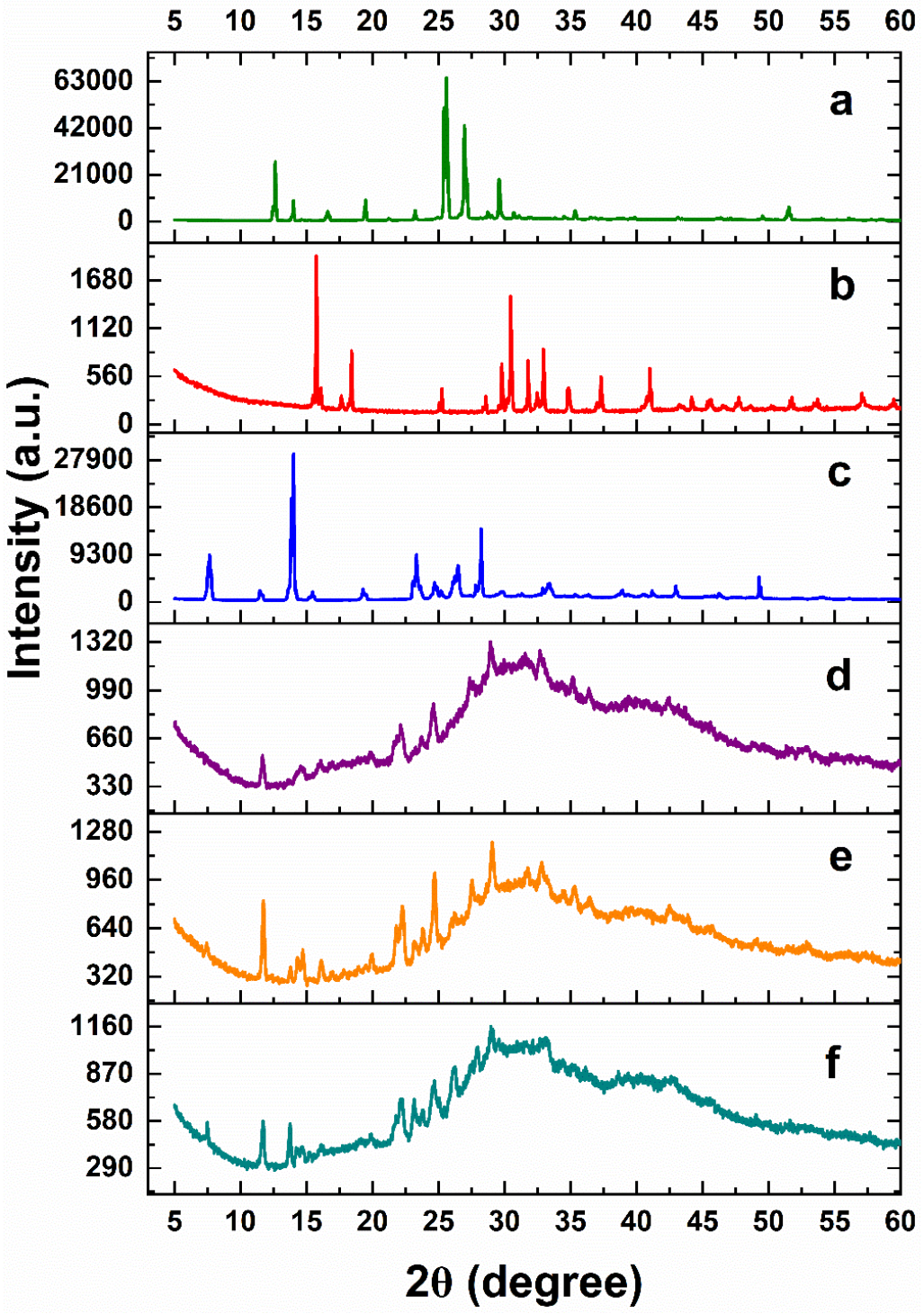

Figure 4.4: P-XRD patterns obtained for a) creatinine, b) $CoCl_2 \cdot 6H_2O$, c) 2-nitrobenzaldehyde, d) C1, e) C2 and f) C3.

In the diffraction pattern of C1 [Figure 4.4 (d)] some new peaks at 2θ = 11.64°, 22.19° and 24.57° were observed, which are not the characteristic peaks of creatinine or

$CoCl_2 \cdot 6H_2O$. Similarly, new diffraction peaks at 2θ = 7.49°, 13.72° and 26.20° were observed for C3 [Figure 4.4 (f)], which are neither the characteristic peaks of any of the reagents nor of C1. Thus, it can be inferred that the P-XRD patterns depict the formation of new compounds as the patterns observed for the products (d, e and f) are unique and not just the mere summations of the diffraction patterns of the reactants (a, b and c). The 2θ range beyond 60° has been discarded as no diffraction peak was observed in this range for any of these entities. Furthermore, from the diffraction patterns, it can be stated that while the reagents are crystalline in nature, the products are largely amorphous. The peak positions and the degree of crystallinity have been presented in Table 4.1 for all the reagents and products. The degree of crystallinity was calculated using the formula:

$$Degree\ of\ crystallinity\ (\%) = \left(\frac{Area\ under\ the\ crystalline\ peaks}{Total\ area}\right) \times 100\% \quad \textbf{(Eq. 4.1)}$$

Table 4.1: P-XRD peak positions and degree of crystallinity obtained for each reactant and product.

Reagent/Product	Peak position (2θ)	Degree of crystallinity (%)
Creatinine	12.63, 14.02, 16.60, 19.44, 23.22, 25.61, 26.87, 28.7, 29.58, 30.71, 35.31, 49.55, 51.63	74.30 %
$CoCl_2.6H_2O$	15.72, 17.67, 18.43, 25.3, 28.64, 29.71, 30.46, 31.79, 32.42, 32.98, 34.81, 37.39, 40.92, 44.13, 45.71, 47.85, 51.82, 53.83, 56.92, 59.44	40.59 %
2-nitrobenzaldehyde	7.59, 11.56, 13.96, 15.41, 19.25, 23.15, 24.67, 25.23, 26.43, 27.75, 28.13, 29.9, 32.79, 33.36, 38.97, 41.11, 42.94, 46.27, 49.36	86.85 %
C1	11.64, 14.54, 16.14, 19.79, 22.19, 23.75, 24.57, 27.35, 28.91, 31.59, 32.66, 35.23, 36.45, 42.43	8.69 %
C2	7.49, 11.79, 13.8, 14.36, 14.73, 16.10, 19.93, 21.75, 22.27, 23.16, 23.83, 24.68, 26.20,	11.76 %

	27.58, 29.06, 31.77, 32.89, 34.42, 35.34, 36.49, 42.46	
C3	7.49, 11.68, 13.72, 14.28, 14.73, 16.06, 19.81, 21.75, 22.15, 23.16, 23.79, 24.64, 25.46, 26.20, 27.87, 28.99, 33.18, 38.64	9.35 %

The higher degree of crystallinity of C2 (11.76 %) as compared to C1 (8.69 %) and C3 (9.35 %) further infers a mixed composition of C2, as it exhibits the characteristic crystalline peaks of both C1 and C3.

4.3.3 Analysis of FTIR and Raman spectra

Figure 4.5 represents the FTIR spectra of the reactants and the products. For creatinine, as seen in spectrum 'a' of Figure 4.5 (B), a peak at 1688 cm^{-1} for C = O stretching was observed. The occurrence of this peak at a lower frequency compared to its typical position, along with lower intensity, can be attributed to the resonance effect as the lone pair of electrons on the adjacent nitrogen atom conjugates with the carbonyl group [30]. The stretching frequency for C = N was observed at 1668 cm^{-1}. The broad bands at 1587 cm^{-1} and 1500 cm^{-1} can be attributed to the bending frequencies for N-H bonds for primary and secondary amines respectively. While, the CH_3 and CH_2 bending peaks occurred at 1456 cm^{-1}, 1434 cm^{-1}, 1418 cm^{-1}, and 1326 cm^{-1}; peaks due to C-N stretching absorptions occurred between 1243 and 1037 cm^{-1}. The absorption peaks at 841 cm^{-1} and 811 cm^{-1} can be attributed to the out-of-plane N-H bending. At higher frequencies, as can be seen in spectrum 'a' of Figure 4.5 (A), C-H stretching at 2808 cm^{-1}, and N-H stretching at 3023 cm^{-1} and 3250 cm^{-1} were also observed. All the IR peaks mentioned above have been designated and reasoned out, strongly in accord with the existing literature [20].

The peaks obtained for $CoCl_2 \cdot 6H_2O$ [spectrum 'b' of Figure 4.5 (A)], are also congruent with its characteristic peaks due to deformational scissor vibration of water, librational vibrations and overtones as reported in the literature [21].

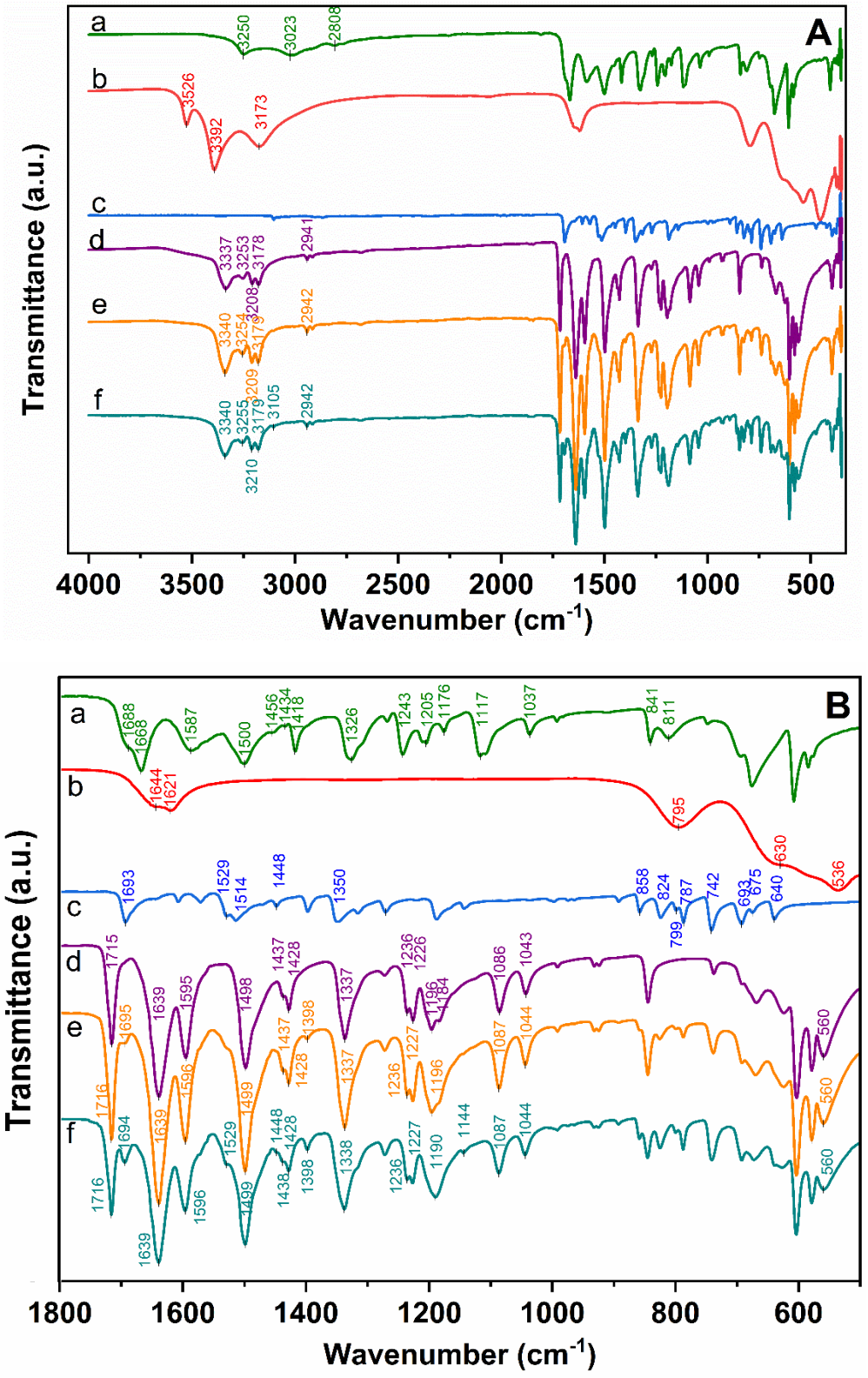

Figure 4.5: FTIR spectra of a) creatinine, b) $CoCl_2 \cdot 6H_2O$, c) 2-nitrobenzaldehye, d) C1, e) C2 and f) C3 in the complete frequency range of 4000–350 cm^{-1} (A) and in the expanded lower frequency range of 1800–500 cm^{-1} (B).

In the spectrum of 2-NBA [spectrum 'c' of Figure 4.5 (B)], a peak at 1693 cm^{-1} for C = O stretching was observed. The effect of conjugation on the carbonyl group of 2-NBA lowered the frequency of the C = O peak, compared to its typical position. The bands at 1514 cm^{-1} and 1350 cm^{-1} of almost equal intensity can be assigned to the respective asymmetric and symmetric stretching of the aromatic -NO_2 group [20]. The C = C present in the aromatic ring, exhibited stretching peaks between 1600 cm^{-1} to 1450 cm^{-1} and the characteristic C = C out-of-the-plane peaks were also observed in the lower frequencies (between 900 cm^{-1} to 650 cm^{-1}) [20].

For C1, as seen in spectrum 'd' of Figure 4.5 (B), the peaks at 1595 cm^{-1} and 1498 cm^{-1} were reproduced for N-H bending for primary and secondary amines respectively, and the intense peak at 1639 cm^{-1} can be designated for C = N stretching. Furthermore, all the characteristic peaks owing to bending in methyl and methylene groups and C-N stretching reappeared but at slightly shifted frequencies. However, unlike in the spectra of creatinine, a sharp and intense peak for C = O at 1715 cm^{-1} was observed. This intensification and shifting of peak to a higher frequency implied that the carbonyl group of creatinine overcomes the resonance effect in the presence of cobalt. This happens because of the formation of a coordinate covalent bond by the lone pair of electrons on the nitrogen atom (at position 3, adjacent to the carbonyl group) of creatinine with the cobalt ion. It is worth noting that depending on the chemical environment, the Co-N stretching can be observed in the entire frequency range from 366 cm^{-1} to 470 cm^{-1} [22]. A prominent peak at 397 cm^{-1} was also observed for C1, as seen in the enlarged IR spectra of the far-infrared region in Figure 4.6, which can be attributed to the Co-N stretching. It is to be noted that a characteristic peak of Co-O stretching at 560 cm^{-1} [23] was also observed. The possibility of coordination of the cobalt ion with the oxygen of the carbonyl group of creatinine is ruled out due to the appearance of an intense C = O stretching peak at its original frequency. Hence, the peak at 560 cm^{-1} can be attributed to the possible coordination of the cobalt ion with the oxygen atom of water molecule (s) from the solvent. At higher frequencies, as can be seen in spectrum 'd' of Figure 4.5 (A), apart from the C-H stretching (2941 cm^{-1}) and N-H stretching (3178 cm^{-1} and 3253 cm^{-1}), a band at 3337 cm^{-1} was also observed for O-H stretching. As the compounds were dried properly and kept in a desiccator before recording the FTIR spectra, the peak at 3337 cm^{-1} further substantiated the formation of the coordination bond of cobalt with water molecule(s).

Hence, it was inferred that the coordination sphere of the creatinine-cobalt complex (C1) comprises the central metal ion, coordinated with creatinine and H_2O.

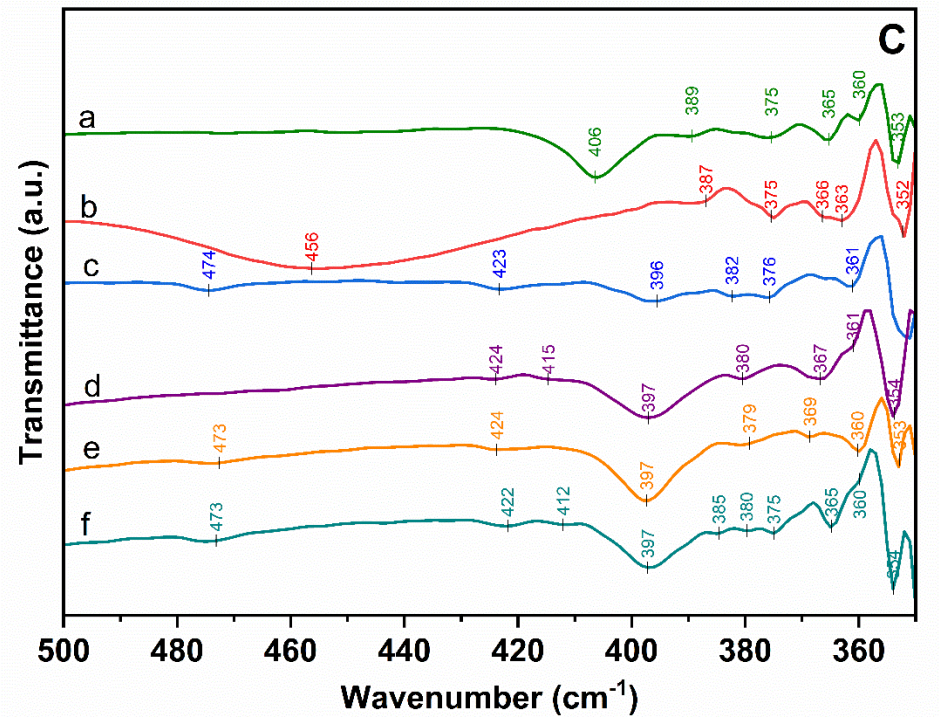

Figure 4.6: FTIR spectra of a) creatinine, b) $CoCl_2 \cdot 6H_2O$, c) 2-nitrobenzaldehye, d) C1, e) C2 and f) C3 in the expanded lower frequency range of 500–350 cm^{-1}.

For C3, as can be seen in spectrum 'f' of Figure 4.5 (B), a prominent peak at 1716 cm^{-1} was observed which can be assigned to the stretching of the C = O group of cobalt-bonded creatinine. Moreover, a peak at 1694 cm^{-1} was also observed, which can be attributed to the stretching of the C = O group (under the conjugation effect) of 2-NBA. As the original peak for C = O stretching in pristine 2-NBA (spectrum 'c') was also observed at a similar position (1693 cm^{-1}), it can be inferred that the carbonyl group of 2-NBA was not involved in any bond formation in C3. In contrast, both the bands for the asymmetric and symmetric stretching of the aromatic -NO_2 group were not observed in C3. This might be due to the chelation of cobalt ions by the oxygen atoms of the nitro group of 2-NBA. As this plausible complex of cobalt ion with 2-NBA in 1:5 water-methanolic solution could not be isolated, it was not possible to determine the oxidation state of cobalt and the possibility of any other ligand, like water molecule, coordinating with the cobalt ion along with 2-NBA. In spectrum 'f' of Figure 4.5 (B), the characteristic

Co-O stretching peak at 560 cm^{-1} was also observed, which further substantiated the chelation between cobalt ions and the nitro group, and/or the coordination of cobalt ions with water molecules (explained in detail in the later sections). The O-H band observed at 3340 cm^{-1}, as seen in spectrum 'f' of Figure 4.5 (A), also inferred the presence of water molecules. At higher frequencies, C-H and N-H stretching peaks were also observed. Hence, it can be stated that the coordination sphere of the creatinine-cobalt-2-NBA complex comprises the central metal ion coordinated with creatinine, 2-NBA and H_2O.

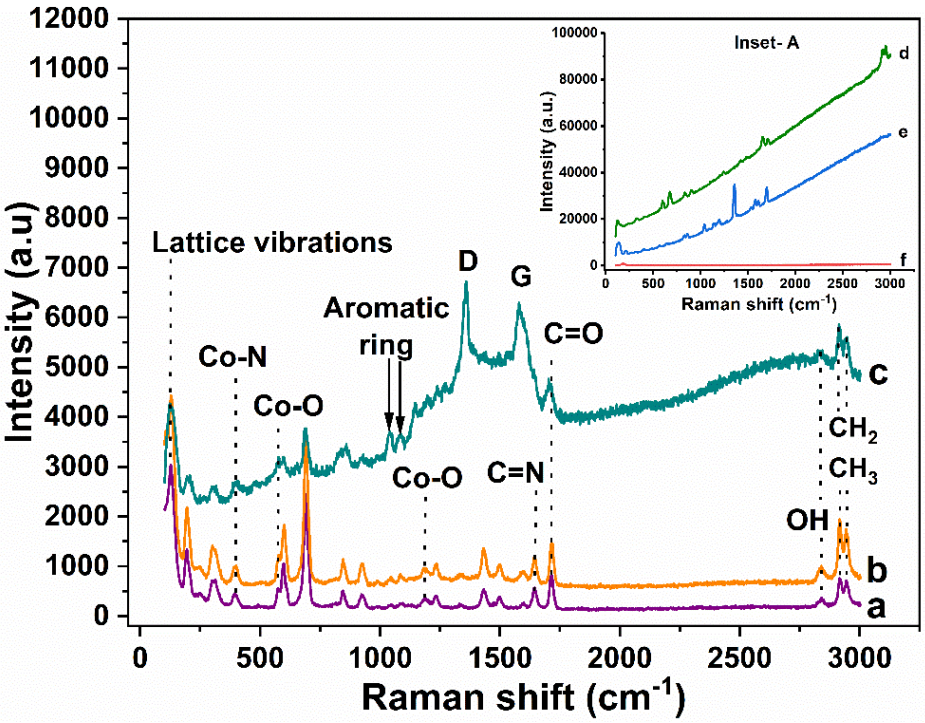

Figure 4.7: Raman spectra obtained for a) C1, b) C2 and c) C3. Inset-A: Raman spectra obtained for d) creatinine, e) 2-nitrobenzaldehyde and f) $CoCl_2 \cdot 6H_2O$.

Raman analysis was also employed to gain additional information about the structures. Figure 4.7 represents the obtained Raman spectra for the products and the reagents. For creatinine, as can be seen in spectrum 'd' of Figure 4.7 (Inset-A), peaks at 1713 cm^{-1} and 1654 cm^{-1} were obtained, which are close to the values reported in the literature for ν(C = O) and ν(C = N), respectively [24, 25]. The peaks at higher frequencies (2918 cm^{-1} and 2852 cm^{-1}) can be attributed to asymmetric stretching of the methylene group and symmetric stretching of the methyl group respectively [26]; while the peaks at lower frequencies in the range of 600–910 cm^{-1} are also the reported characteristic peaks

of creatinine [27]. For 2-NBA, as can be seen in spectrum 'e' of Figure 4.7 (Inset-A), characteristic peaks for $\nu(NO_2)$ at 1355 cm^{-1} [28], and for $\nu(C = O)$ at 1700 cm^{-1} were observed, in addition to some weak peaks for the aromatic ring. For $CoCl_2 \cdot 6H_2O$, represented by spectrum 'f' of Figure 4.7 (Inset-A), only a low-intensity peak due to lattice vibration was observed at 181 cm^{-1}.

The analysis of the Raman spectra of the products substantiated the inferences drawn from the FITR analyses and provided some additional structural information. For C1, represented by spectrum 'a' of Figure 4.7, besides the characteristic peaks for $\nu(C = O)$ and $\nu(C = N)$, some additional peaks at 570 cm^{-1} and 1182 cm^{-1} which are close to the reported values for ν(Co-O) [29], and also at 405 cm^{-1} which is close to the reported value for ν(Co-N) [30], were observed. At higher frequencies, apart from bands for the methylene and the methyl group, a weak peak at 2840 cm^{-1} was observed, which is in the range for characteristic ν(OH) stretching mode [31]. All these aforementioned characteristic peaks were also observed for C3, as seen in spectrum 'c' of Fig. 4. However, the intense Raman peak for the $\nu(NO_2)$ was not observed in C3, further substantiating the coordination of the nitro group of 2-NBA with cobalt ion in C3. In addition, 'D band' and 'G band' at 1360 cm^{-1} and 1580 cm^{-1} respectively were also observed [32], which implied a graphitic structure of the creatinine-cobalt-2-NBA complex and hence, also explained the flaky appearance of the complex. The graphitic structure might have resulted from the stacking of the aromatic rings of 2-NBA, forming π-π interactions.

Due to the heterogeneous mixture composition of C2, its FTIR spectrum (spectrum 'e', Figure 4.5) appeared similar to that of C3 (spectrum 'f', Figure 4.5), while its Raman spectrum (spectrum 'b', Figure 4.7) closely resembled the spectrum of C1 (spectrum 'a', Figure 4.7). Hence, C2 was excluded from any further analysis.

4.3.4 Analysis of DRS

Figure 4.8 represents the diffuse reflectance spectra obtained for the reactants and products. In the spectrum of creatinine (spectrum 'a'), an absorbance at 236 nm was observed which can be attributed to the π-π^* transition of the carbonyl group of creatinine. Typically, the π-π^* transition of the carbonyl group occurs at a wavelength lower than 200 nm but due to the presence of an auxochrome (secondary amine group) with a lone pair of electrons on the nitrogen atom, adjacent to the carbonyl group, a bathochromic shift in the

transition occurred. However, in the spectrum of C1 (spectrum 'd'), the strong π-π* transition could not be observed. This can be due to the involvement of the lone pair of electrons on the nitrogen atom of creatinine in coordination with the cobalt ion, which shifted the λ_{max} of the π-π* transition to its typical position (below our cut-off point). In the electronic spectrum of 2-NBA (spectrum 'c'), the primary bands of the aromatic ring (due to π-π* transitions) were observed at 226 nm and 255 nm. The appearance of these primary bands at higher wavelengths was caused by the two electron-withdrawing groups ortho to each other in 2-nitrobenzaldehyde. These primary bands were also observed for C3 (at 224 nm and 252 nm) as seen in spectrum 'e'. This confirmed the presence of a substituted aromatic ring in the creatinine-cobalt-2-NBA complex.

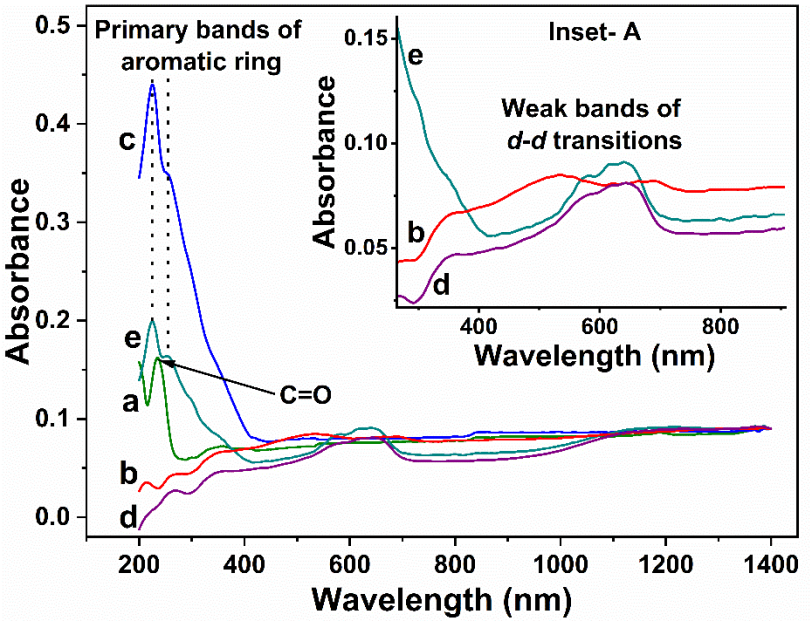

Figure 4.8: UV-visible DRS obtained for a) creatinine, b) $CoCl_2 \cdot 6H_2O$, c) 2-nitrobenzaldehye, d) C1, e) C3 (Inset- A: Enlarged view of the d-d transitions occurring in 'b', 'd' and 'e').

In Inset-A of Figure 4.8, weak bands of *d-d* transitions in $CoCl_2 \cdot 6H_2O$ and the two cobalt complexes can be observed, most likely, due to spin-forbidden transitions from lower to higher energy levels. *Mishra et al.* [33] presented the DRS analysis of hydrated cobalt chloride with H_3BO_3 and $MgCO_3$ as the reference standards and reported that the resolution and the position of the peaks varied with the standards. With $BaSO_4$ as the reference standard, we obtained some *d-d* transition peaks for $CoCl_2 \cdot 6H_2O$ at 353 nm, 536 nm, and 693 nm, as seen in its spectrum (spectrum 'b'). These peak positions are very

close to the reported values for non-calcined $CoCl_2.xH_2O$ (392.2 nm, 540 nm, and 693.7 nm with $MgCO_3$ as reference standard; 350.7 nm, 540.5 nm, and 686.5 nm with H_3BO_3 as reference standard) and hence, the peaks can be assigned for ^2E_g (H) ← $^4T_{1g}$, $^4T_{1g}$ (P) ← $^4T_{1g}$, and $^2T_{1g}$ (H) ← $^4T_{1g}$ respectively [33].

The DRS of C1, represented by spectrum 'd', showed a similar trend as $CoCl_2 \cdot 6H_2O$. It indicated the presence of weak field ligands and a d^7 configuration of the cobalt ion in the creatinine-cobalt complex. For C1, while the ^2E_g (H) ← $^4T_{1g}$ transition was observed at the same position (353 nm), the peaks for $^4T_{1g}$ (P) ← $^4T_{1g}$, and $^2T_{1g}$ (H) ← $^4T_{1g}$ occurred at shifted positions (582 nm and 655 nm, respectively). This can be due to structural changes in the ligand environment.

In the DRS of C3, as can be seen in spectrum 'e', the peaks did not appear well-resolved, as peaks observed at 543 nm, 579 nm, 614 nm and 639 nm were seemingly overlapping. Another peak was observed at 301 nm, which appeared as a shoulder peak due to the presence of the nearby intense primary bands of the aromatic ring. This indicated a different *d*-configuration of the cobalt ion in the creatinine-cobalt-2-NBA complex.

4.3.5 Elemental compositions and molecular formulas of the complexes: EDX analysis

EDX spectra were recorded for the two prepared complexes, C1 and C3 as shown in Figure 4.9. Coupled with the information gathered from the previous analyses about the ligands coordinating with the cobalt ions in the complexes, the analysis of the elemental compositions enabled us to deduce the formulas of the C1 and C3 as $[Co(CR)_3(H_2O)]Cl_2$ (molar mass: 487.19 g/mol) and $[Co(CR)_3(H_2O)_2(2\text{-NBA})]Cl_3$ (molar mass: 691.76 g/mol) respectively, where CR = creatinine. The comparison of experimental and theoretical elemental compositions for the complexes has been presented in Table 4.2, which concluded that the proposed molecular formula of the complexes well-satisfied the experimental EDX data. As the spatial arrangement of the ligands around the central metal ion requires more complex analyses and is beyond the scope of our present objective, simple two-dimensional representations of the coordination spheres of the synthesized complexes have been proposed, as shown in Scheme 4.1.

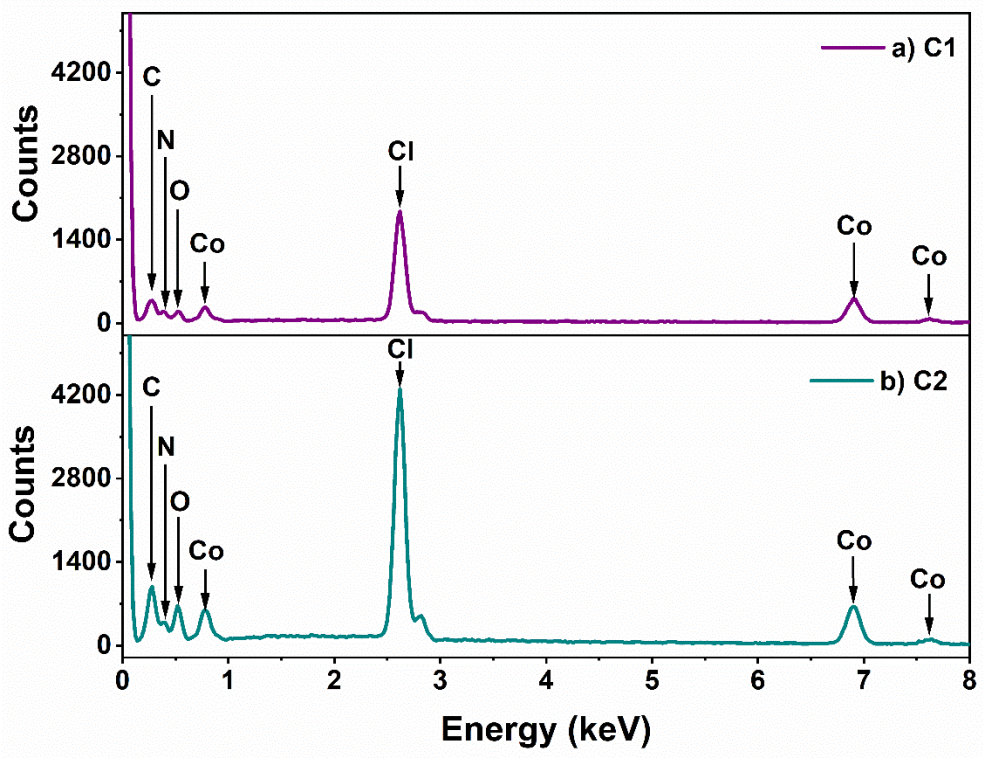

Figure 4.9: EDX spectra obtained for a) C1 and b) C3.

Table 4.2: Comparison of experimental and theoretical weight % of elements (C, N, O, Cl and Co) in the prepared cobalt complexes.

Element	**$[Co(CR)_3(H_2O)]Cl_2$**		**$[Co(CR)_3(H_2O)_2(2\text{-}NBA)]Cl_3$**	
	Experimental weight %	Theoretical weight %	Experimental weight %	Theoretical weight %
C	31.38	31.02	34.60	34.45
N	27.31	27.14	21.37	21.15
O	13.42	13.78	18.98	19.34
Cl	15.15	15.27	15.80	16.07
Co	12.75	12.69	9.26	8.90

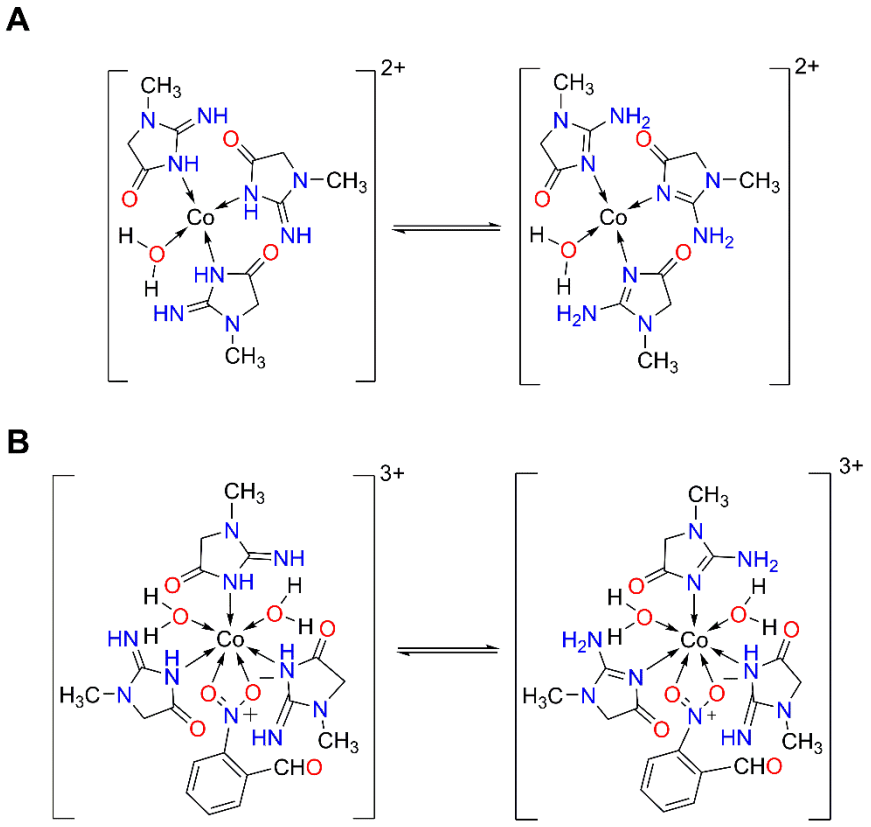

Scheme 4.1: Structural representation of the coordination sphere of A) creatinine-cobalt complex, and B) creatinine-cobalt-2-NBA complex, having isomeric forms of creatinine.

4.3.6 Electrochemical analysis

Electrochemical analysis was done to confirm the oxidation states of the central metal ions in both the complexes and the voltammogram responses are shown in Figure 4.10. The CVs and DPVs were recorded by starting from the negative potential (− 1.5 V). It can be seen in curve 'a' of Figure 4.10 (A) that three major oxidation peaks (Ox_{a0}, Ox_{a1} and Ox_{a2}), two shoulder oxidation peaks of low intensity (Ox_{a3} and Ox_{a4}) and a reduction peak (R_{a1}) were observed in the CV of cobalt chloride solution. While Ox_{a0} (at − 0.62 V) can be attributed to the dissolution of free Co^{2+} ions from the electrode surface, the other two major oxidation peaks can be assigned for Co^{3+}/Co^{2+} (Equation 4.2) and Co^{4+}/Co^{3+} (Equation 4.3) redox processes. This is in agreement with a previously reported finding [34].

Ox_{a1} (at 0.05 V): $Co^{2+} \rightarrow Co^{3+} + 1e^-$

(Eq. 4.2)

Ox_{a2} (at 1.25 V): $Co^{3+} \rightarrow Co^{4+} + 1e^-$

(Eq. 4.3)

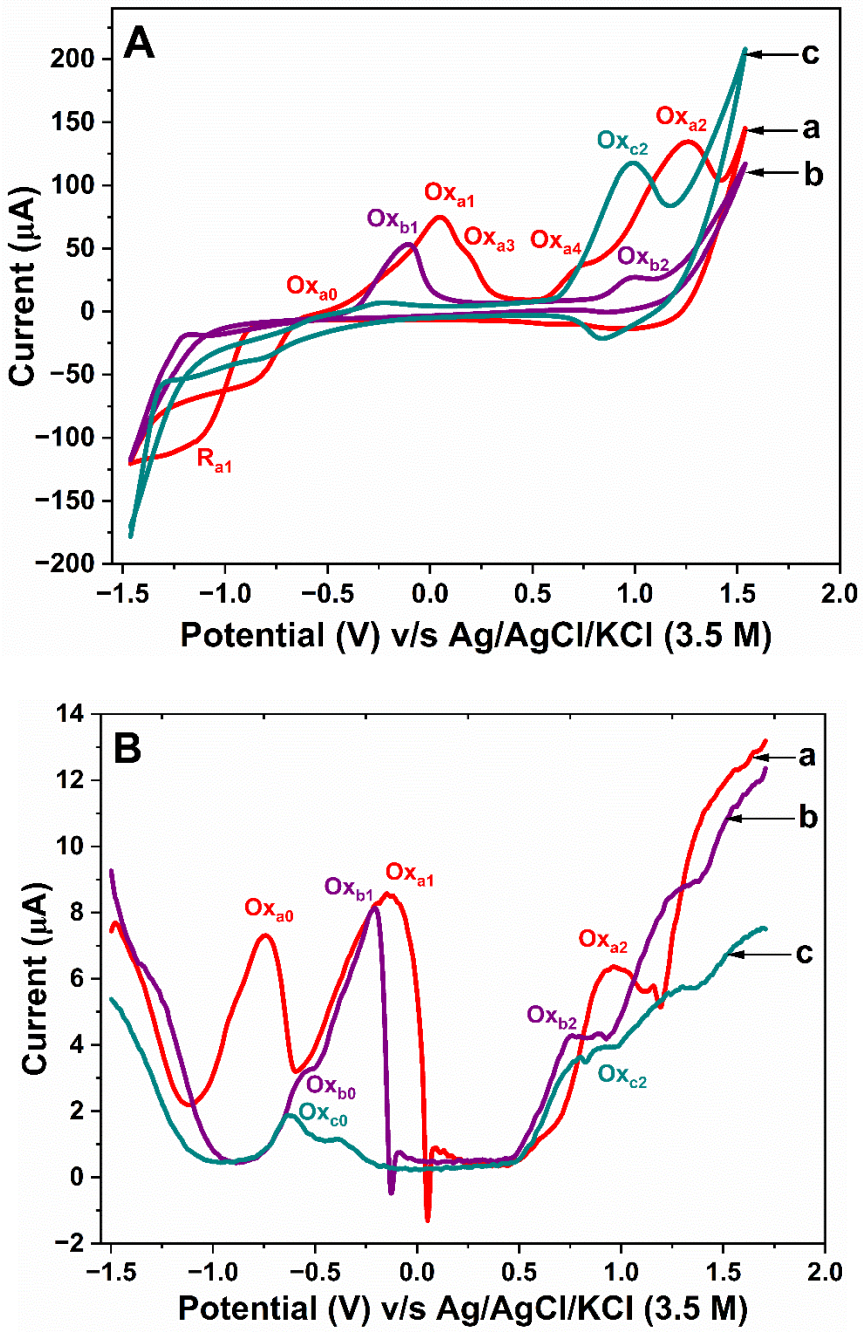

Figure 4.10: A) CVs and B) DPVs obtained for aqueous solutions of a) cobalt chloride b) $[Co(CR)_3(H_2O)]Cl_2$ and c) $[Co(CR)_3(H_2O)_2(2\text{-NBA})]Cl_3$.

It was observed that the peak current for Ox_{a1} decreased, while that of Ox_{a2} increased with consecutive cycles until saturation was reached. This observation indicated the gradual decrease of free Co^{2+} ions, due to the irreversibility of Ox^{a1}, and the gradual increase of Co^{3+} ions, produced in Ox_{a1} and via the reversal of Ox_{a2} (reduction peak, R_{a1} at − 1.13 V).

It was also noted that, unlike the intensities of the major oxidation peaks, the intensities of the two shoulder oxidation peaks, Ox_{a3} (at 0.20 V) and Ox_{a4} (at 0.72 V), remain unaltered with the increase in the concentration of the cobalt chloride solutions. It can be inferred that these low-intensity peaks, which cannot be considered for analysis, are due to oxidation of the trace amount of cobalt-oxides formed in the solution [35].

The curve 'b' of Figure 4.10 (A) represents the CV of the aqueous solution of $[Co(CR)_3(H_2O)]Cl_2$. As cobalt carries an oxidation state of +2 in this complex, accordingly only two oxidation peaks Ox_{b1} (at − 0.10 V) and Ox_{b2} (at 0.98 V) were observed for $Co^{2+} \rightarrow Co^{3+}$ and $Co^{3+} \rightarrow Co^{4+}$ respectively. Furthermore, as the cobalt ions were coordinated to ligands, no oxidation peak was observed due to the dissolution of free Co^{2+} ions from the electrode surface. The coordinated nature of the Co^{2+} ion in this complex also justifies the slight shift in the oxidation peaks to lower potentials, as compared to the free Co^{2+} ion.

The curve 'c' of Figure 4.10 (A) represents the CV of the aqueous solution of $[Co(CR)_3(H_2O)_2(2\text{-NBA})]Cl_3$, where we can observe only one oxidation peak Ox_{c2} (at 0.98 V) which can be attributed to the $Co^{3+} \rightarrow Co^{4+}$ oxidation. This inferred that the oxidation state of cobalt in this complex is +3, a finding which is in line with the conclusions drawn in the previous sections.

In the same curve 'c', a low-intensity peak at 0.83 V was observed during the reverse scan, which can be attributed to structural rearrangements around the working electrode surface to counter the effect of high potentials. However, no prominent reduction peak was observed for both complexes, indicating the irreversibility of the oxidation processes of the cobalt complexes, which was in contrast with the system containing free cobalt ions.

Similar results were obtained for the DPVs of the solutions, as seen in Figure 4.10 (B). However, due to the higher sensitivity of DPV as compared to CV, additional oxidation peaks, Ox_{b0} (at − 0.55 V) and Ox_{c0} (at − 0.61 V), were observed for

$[Co(CR)_3(H_2O)]Cl_2$ (curve 'b') and $[Co(CR)_3(H_2O)_2(2\text{-NBA})]Cl_3$ (curve 'c') respectively. These oxidation peaks can be attributed to the dissolution of their respective cationic sphere from the electrode surface.

In the previous chapter, a prominent oxidation peak for creatol (2- Amino-5-hydroxy-1-methyl-1,5-dihydro-4 H-imidazole-4-one), which is an oxidized product of creatinine by 2-NBA under strong basic conditions, was observed at 0.69 V [24]. However, no creatol oxidation peak was observed in the voltammogram of these cobalt complexes, proving that the oxidation of creatinine by 2-NBA does not occur in the absence of a strong base.

4.3.7 Yield and physiochemical properties: magnetism, conductivity and solubility

The yield of $[Co(CR)_3(H_2O)]Cl_2$ and for $[Co(CR)_3(H_2O)_2(2\text{-NBA})]Cl_3$ were calculated to be 73.18% and 86.34%, as presented in Table 4.3. As creatinine molecules were responsible for the major weight % of the complexes, while cobalt and 2-nitrobenzaldehyde were in excess, the theoretical yields of the complexes were calculated considering the total use-up of 75 mg of creatinine in complex formation.

Table 4.3: Yield percentage calculated for the cobalt complexes.

Complex	**A = Theoretical yield (mg)**	**B = Actual yield (mg)**	**Percent Yield = (A/B)*100 %**
$[Co(CR)_3(H_2O)]Cl_2$	107.67	78.80	73.18 %
$[Co(CR)_3(H_2O)_2(2\text{-NBA})]Cl_3$	152.88	132.00	86.34 %

As both the prepared cobalt complexes are amorphous and have no definite long-range geometry, the exact splitting of the *d*-orbitals in the ligand environment cannot be known. Nonetheless, the EPR spectra of the complexes, as presented in Figure 4.11, demonstrated that both complexes are paramagnetic in nature. 'Inset-A' in Figure 4.11 shows multiple hyperfine splitting of the spectra in the selected range of 577–677 mT. In the paramagnetic cobalt complexes, due to the presence of several nuclei of H, N and Co, with respective nuclear spins of 1/2, 1 and 7/2, complicated hyperfine interactions can be expected, which are difficult to comprehend or predict precisely. However, the different patterns of hyperfine splitting observed for the complexes inferred the change in their local

environment. A similar pattern was also obtained in the EPR spectra of a previously reported paramagnetic complex of cobalt with N-donor ligand [36].

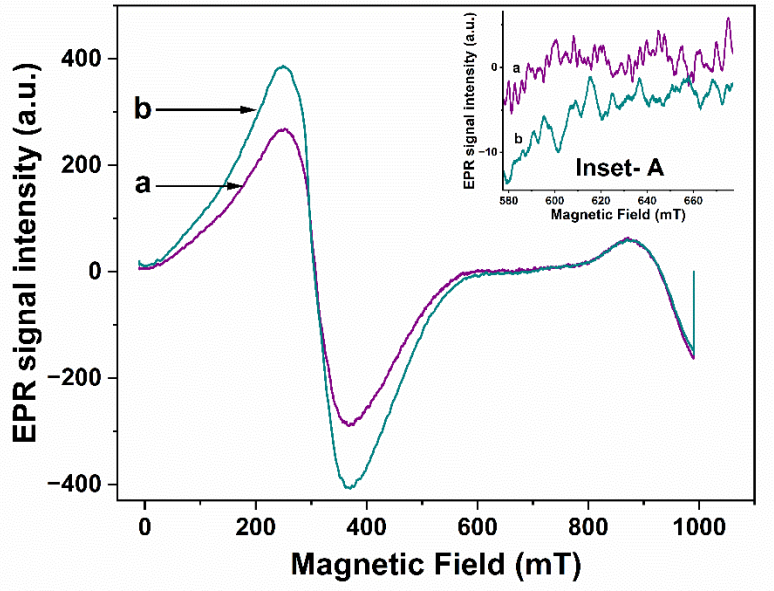

Figure 4.11: EPR spectra obtained for a) $[Co(CR)_3(H_2O)]Cl_2$, and b) $[Co(CR)_3(H_2O)_2(2\text{-NBA})]Cl_3$. [Inset-A: Enlarged EPR spectra of 'a' and 'b' in the magnetic field range of 577-677 mT].

The solubilities of the complexes were tested in different mediums and both complexes exhibited similar responses. Both complexes were found to be sparingly soluble in acetonitrile and ethanol, but insoluble in acetone. In water, while $[Co(CR)_3(H_2O)]Cl_2$ is readily soluble on gentle shaking to give a pink-coloured solution, $[Co(CR)_3(H_2O)_2(2\text{-NBA})]Cl_3$ is soluble upon vigorous shaking to form a brown-coloured solution. The difference in the colour of the aqueous solutions of the complexes also indicated a difference in the oxidation states of the central metal ions in the two complexes, as was inferred by their EDX and electrochemical analyses. $AgNO_3$ test was performed to establish the presence of chloride ions as the counterion in the complexes. When a few drops of dilute $AgNO_3$ were added to the aqueous solutions of the complexes, white precipitates were formed instantly, thus confirming the presence of chloride outside the coordination sphere. The colouration of aqueous solutions of the complexes and the formation of white precipitates during the $AgNO_3$ test have been shown in Figure 4.12.

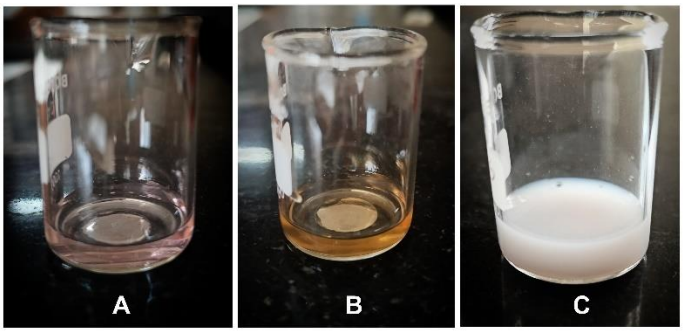

Figure 4.12: A) Pink-coloured aqueous solution of $[Co(CR)_3(H_2O)]Cl_2$, B) brown-coloured aqueous solution of $[Co(CR)_3(H_2O)_2(2\text{-NBA})]Cl_3$, and C) white precipitate obtained on adding drops of $AgNO_3$ solution to aqueous solution of the cobalt complex.

Table 4.4: Conductivity measured for KCl, $CoCl_2.6H_2O$, $[Co(CR)_3(H_2O)]Cl_2$ and $[Co(CR)_3(H_2O)_2(2\text{-NBA})]Cl_3$.

Compound/Complex	**No. of moles of compound/complex**	**No. of moles of dissociated cations**	**No. of moles of dissociated Cl^-**	**Total no. of dissociated ions**	**Conductivity (µS/m)**
KCl	60.33×10^{-6}	60.33×10^{-6}	60.33×10^{-6}	120.66×10^{-6}	920
$CoCl_2.6H_2O$	18.91×10^{-6}	18.91×10^{-6}	37.92×10^{-6}	56.83×10^{-6}	470
$[Co(CR)_3(H_2O)]Cl_2$	9.23×10^{-6}	9.23×10^{-6}	18.46×10^{-6}	27.69×10^{-6}	390
$[Co(CR)_3(H_2O)_2(2\text{-NBA})]Cl_3$	6.50×10^{-6}	6.50 × 10-6	19.50×10^{-6}	26×10^{-6}	290

The conductivities of the complexes in aqueous medium were measured at room temperature (21 °C) and compared with aqueous solutions of KCl and $CoCl_2 \cdot 6H_2O$, as presented in Table 4.4. All these prepared solutions have the same w/v% (4.5 mg in 10 ml). An expected sharp decrease in the conductivity of cobalt chloride (470 µS/m), as compared

to potassium chloride (920 μS/m) was observed, because of the reduction in the number of moles of dissociated ions in the former case. The measured conductivities of the complexes confirmed the formation of ionic complexes and are comparable to that of cobalt chloride. These complexes exhibited a lower conductivity as compared to cobalt chloride due to the lower numbers of dissociated ions. It can also be understood from the conductivity table that both the complexes have a comparable number of moles of chloride ions and hence, the contribution towards conductivity by the anionic species would be similar. However, the decrease in conductivity for $[Co(CR)_3(H_2O)_2(2\text{-NBA})]Cl_3$ (290 μS/m) as compared to $[Co(CR)_3(H_2O)]Cl_2$ (390 μS/m) can be attributed to the lower number of moles of the dissociated cationic sphere of the former, as well as its bulkier nature.

4.3.8 Brown filtrate analysis

The brown filtrate that was obtained during the preparation process of the creatinine-cobalt complex in the presence of 2-nitrobenzaldehyde was collected in a Petri dish, covered carefully with pricked parafilm and air-dried at room temperature. After 3 weeks, the filtrate dried out and needle-like crystals were obtained. From preliminary investigation using a single crystal-XRD, the lattice parameters of the crystals were determined as a = 11.45 Å, b = 3.99 Å, and c = 7.59 Å, which matched with the reported characteristic crystallographic constants of 2-nitrobenzaldehyde [37]. Hence, it was confirmed that the filtrate contained unreacted 2-nitrobenzaldehyde and thus, no more crystallographic data was collected.

4.4 Conclusion

In this chapter, we have reported two new complexes, $[Co(CR)_3(H_2O)]Cl_2$ (% yield = 73.18%) and $[Co(CR)_3(H_2O)_2(2\text{-NBA})]Cl_3$ (% yield = 86.34%). While the former complex is rod-shaped and dark blue in colour, the latter is of nano-fibrous morphology and light blue. However, in both complexes, the CR-cobalt ratio of 3:1 is maintained. As concluded from their P-XRD patterns, both complexes are largely amorphous with the degree of crystallinity calculated to be 8.69% and 9.65% respectively. The coordination of the cobalt ions with the endocyclic nitrogen of creatinine, its chelation with the nitro group of 2-NBA in the complexes, and the presence of H_2O molecules in the coordination spheres were determined by the FTIR and Raman spectra. Raman spectra further established the

graphitic structure of $[Co(CR)_3(H_2O)_2(2\text{- NBA})]Cl_3$. DRS analysis hinted at the different *d*-configurations of the complexes, while from EDX and electrochemical analyses, the oxidation states of the complexes were determined to be +2 and +3 respectively. Both complexes are water-soluble, ionic, electrochemically active, conducting and paramagnetic. However, it has been established that the oxidation states of the central metal ion, morphological characteristics, and the number/type of coordinating ligands in the creatinine-cobalt complex can be altered by the addition of 2-nitrobenzaldehyde in the reaction pathway. It can also be comprehended that Co^{2+} coordinates instantaneously with creatinine. 2-NBA can be introduced into the coordinating sphere of the creatinine-cobalt complex by its prior coordination with cobalt ion. This explored coordination pathway promises a strong base for designing an electrochemical creatinine sensor for monitoring renal dysfunctions.

References

1. Mitewa, M. Coordination properties of the bioligands creatinine and creatine in various reaction media. *Coordination Chemistry Reviews*, 140:1–25, 1995.

2. Mitewa, M., Bontchev, P. R. and Kabassanov, K., 1985. A four-membered chelate complex of Cu (II) with creatinine. *Polyhedron*, 4(7):1159–1161, 1985.

3. Udupa, M. R. and Krebs, B. Crystal and molecular structure of creatininium tetrachlorocuprate (II). *Inorganica Chimica Acta*, 33:241–244, 1979.

4. Mitewa, M., Gencheva, G., Ivanova, I., Zhecheva, E. and Mechandjiev, D. Complex formation of monomeric and dimeric copper (II) complexes with creatinine in organic media. *Polyhedron*, 10(15):1767–1771, 1991.

5. Muralidharan, S., Nagaraja, K. S. and Udupa, M. R. Cobalt (II) complexes of creatinine. *Transition Metal Chemistry*, 9:218–220, 1984.

6. Gencheva, G., Mitewa, M. and Bontchev, P. R. Dimeric and oligomeric platinum (II, II),(II, III) and palladium (II, II) complexes with creatinine. *Polyhedron*, 11(18):2357–2361, 1992.

7. Mitewa, M., Gencheva, G., Bontchev, P. R., Zhecheva, E. and Nefedov, V. Structure of Ni (II)-creatinine complex species formed in non-aqueous media. *Inorganica Chimica Acta*, 164(2):201–204, 1989.

8. Muralidharan, S., Nagaraja, K. S. and Udupa, M. R. Creatinine complexes of zinc, cadmium and mercury. *Polyhedron*, 3(5):619–621, 1984.

9. Canty, A. J., Fyfe, M. and Gatehouse, B. M. Organometallic compounds containing a guanidinium group. Phenylmercury (II) derivatives of creatine and creatinine. *Inorganic Chemistry*, 17(6):1467–1471, 1978.

10. Gangopadhyay, D., Singh, S. K., Sharma, P., Mishra, H., Unnikrishnan, V. K., Singh, B. and Singh, R. K. Spectroscopic and structural study of the newly synthesized heteroligand complex of copper with creatinine and urea. *Spectrochimica Acta Part A: Molecular and Biomolecular Spectroscopy*, 154:200–206, 2016.

11. El-Sayed, M. Y., Refat, M. S., Altalhi, T., Eldaroti, H. H. and Alam, K. Preparation, spectroscopic, thermal and molecular docking studies of covid-19 protease on the manganese (II), iron (III), chromium (III) and cobalt (II) creatinine complexes. *Bulletin of the Chemical Society of Ethiopia*, 35(2):399–412, 2021.

12. Younes, A. A., Alsuhaibani, A. M. and Refat, M. S. Preparation, spectroscopic and thermal studies on the zinc (II), cadmium (II), tin (II), lead (II) and antimony (III) creatinine complexes. *Bulletin of the Chemical Society of Ethiopia*, 36(4):831–842, 2022.

13. Van Pilsum, J. F., Martin, R. P., Kito, E. and Hess, J. Determination of creatine, creatinine, arginine, guanidinoacetic acid, guanidine, and methylguanidine in biological fluids. *Journal of Biological Chemistry*, 222:225–236, 1956.

14. Hussain, N., Puzari, P. A novel method for electrochemical determination of creatinine in human urine based on its reaction with 2-nitrobenzaldehyde using a glassy carbon electrode. *Journal of Applied Electrochemistry*, 54:175–187, 2024.

15. El-Sayed, L. and Ragsdale, R. O. Chelating nitrite groups in some cobalt (II) complexes. *Inorganic Chemistry*, 6(9):1644–1646, 1967.

16. Goodgame, D. M. L. and Hitchman, M. A. Studies of nitro and nitrito complexes. II. Complexes containing chelating NO_2 groups. *Inorganic Chemistry*, 4(5):721–725, 1965.
17. Eaton, D. R., Majid, A. and Tong, J. P. K. Cobalt (II) and zinc (II) complexes of thiourea as catalysts for the reactions between carbonyl compounds and anilines. *Inorganica Chimica Acta*, 61:25–31, 1982.
18. Mizuno, J. An X-ray study on the structure of cobalt dichloride hexahydrate. *Journal of the Physical Society of Japan*, 15(8):1412–1420, 1960.
19. Li, W., Shi, W., Nan, W., Fei, Z., Cheng, C. and Zhao, H. Solid-liquid phase equilibrium and thermodynamic functions: 2-Nitrobenzaldehyde in different neat solvents and ternary system of 2-nitrobenzaldehyde+ 4-nitrobenzaldehyde+ ethyl acetate. *Journal of Molecular Liquids*, 250:171–181, 2018.
20. Pavia, D. L., Lampman, G. M., Kriz, G. S., and Vyvyan, J. R., 2015. *Introduction to spectroscopy*. Cengage Learning, Boston, MA, 2008.
21. Netskina, O. V., Pochtar, A. A., Komova, O. V. and Simagina, V. I. Solid-state $NaBH_4$ composites as hydrogen generation material: effect of thermal treatment of a catalyst precursor on the hydrogen generation rate. *Catalysts*, 10(2):201, 2020.
22. Thornton, D. A. and Verhoeven, P. F. Substituent Effects on the Cobalt–Nitrogen Stretching Frequencies in the Far–Infrared Spectra of Cobalt (II) Chloride Complexes of Substituted Anilines. *Spectroscopy Letters*, 28(4):587–594, 1995.
23. Fouad, O. A., Makhlouf, S. A., Ali, G. A. and El-Sayed, A. Y. Cobalt/silica nanocomposite via thermal calcination-reduction of gel precursors. *Materials Chemistry and Physics*, 128(1-2):70–76, 2011.
24. Dong, M., Zhang, Q., Xing, X., Chen, W., She, Z. and Luo, Z. Raman spectra and surface changes of microplastics weathered under natural environments. *Science of the Total Environment*, 739:139990, 2020.
25. Nandi, R., Singh, H. K., Singh, S. K., Rao, D. S., Prasad, S. K., Singh, B. and Singh, R. K. Investigation of liquid crystalline property of a new calamitic liquid crystalline system methyl 4-(4′-(4″-(decyloxy) benzyloxy) benzylideneamino) benzoate. *Liquid Crystals*, 44(7):1185–1193, 2017.
26. Arias, J. M., Tuttolomondo, M. E., Díaz, S. B. and Altabef, A. B. FTIR and Raman analysis of l-cysteine ethyl ester HCl interaction with

dipalmitoylphosphatidylcholine in anhydrous and hydrated states. *Journal of Raman Spectroscopy*, 46(4):369–376, 2015.

27. Saatkamp, C. J., de Almeida, M. L., Bispo, J. A. M., Pinheiro, A. L. B., Fernandes, A. B. and Silveira Jr, L. Quantifying creatinine and urea in human urine through Raman spectroscopy aiming at diagnosis of kidney disease. *Journal of Biomedical Optics*, 21(3):037001, 2016.
28. Quaroni, L. and Smith, W.E. The nitro stretch as a probe of the environment of nitrophenols and nitrotyrosines. *Journal of Raman Spectroscopy*, 30(7):537–542, 1999.
29. Holze, R. Surface Raman spectroelectrochemical studies of oxygen reduction catalysts: Co—tetramethoxyphenylporphyrin. *Electrochimica Acta*, 36(5-6):999–1007, 1991.
30. Dong, S., Padmakumar, R., Banerjee, R. and Spiro, T.G. Co− C bond activation in B_{12}-dependent enzymes: cryogenic resonance raman studies of methylmalonyl-coenzyme a mutase. *Journal of the American Chemical Society*, 121(30):7063–7070, 1999.
31. Ruan, H. D., Frost, R. L. and Kloprogge, J. T. Comparison of Raman spectra in characterizing gibbsite, bayerite, diaspore and boehmite. *Journal of Raman Spectroscopy*, 32(9):745750, 2001.
32. Garg, P., Bharti, Soni, R. K. and Raman, R. Graphene oxide–silver nanocomposite SERS substrate for sensitive detection of nitro explosives. *Journal of Materials Science: Materials in Electronics*, 31:1094–1104, 2020.
33. Mishra, S.K. and Kanungo, S.B. Thermal dehydration and decomposition of cobalt chloride hydrate ($CoCl_2 \cdot xH_2O$). *Journal of Thermal Analysis*, 38:2437–2454, 1992.
34. Chai, L. Q., Huang, J. J., Zhang, H. S., Zhang, Y. L., Zhang, J. Y. and Li, Y. X. An unexpected cobalt (III) complex containing a Schiff base ligand: Synthesis, crystal structure, spectroscopic behavior, electrochemical property and SOD-like activity. *Spectrochimica Acta Part A: Molecular and Biomolecular Spectroscopy*, 131:526–533, 2014.
35. Makarava, I., Vänskä, J., Kramek, A., Ryl, J., Wilson, B. P., Yliniemi, K. and Lundström, M. Electrochemical cobalt oxidation in chloride media. *Minerals Engineering*, 211:108679, 2024.

36. Miecznikowski, J. R., Zygmont, S. E., Jasinski, J. P., Kaur, M., Almanza, E., Kharbouch, R. M., Bonitatibus, S. C., Mircovich, E. E., Le Magueres, P., Reinheimer, E. and Weitz, A. C. Synthesis, characterization, and electrochemistry of SNS cobalt (II) tridentate complexes. *Transition Metal Chemistry*, 47(2):127–137, 2022.

37. Coppens, P. and Schmidt, G. M. J. X-ray diffraction analysis of o-nitrobenzaldehydes. *Acta Crystallographica*, 17(3):222–228, 1964.